I. Troch, F. Breitenecker, eds. ISBN 978-3-901608-35-3

THE MULTIPHYSICS MODEL OF THE GAS-DAMPED MICROMIRROR FOR THE MEMS-BASED OPTICAL SWITCH

I. Plander[1], M. Stepanovsky[1]
[1]Alexander Dubcek University of Trencin, Trencin, Slovakia;

Corresponding Author: I. Plander, Alexander Dubcek University of Trencin, Department of Informatics
Studentska 2, 911 50 Trencin, Slovakia; plander@tnuni.sk

Abstract. The multiphysics model with distributed parameters of a gas-damped micromirror and its solution by the finite element method (FEM) is presented. The model is a useful tool for micromirror design and optimization (i.e., the optimization of the shape and dimensions of the micromirror, and its control circuits). The MEMS-based micromirrors have been already fabricated and can be used in the optical crossconnects in all-optical high-throughput interconnection networks [1–5]. Many researchers and companies labour for reducing switching time of the switch because for useful application in all-optical networks it is necessary to achieve short switching time as much as possible, i.e. the micromirror have to adopt new steady-state position in minimal time. Our approach is based on the presence of suitable gas, which can cause aperiodic transient response and thus improve the properties of the switch. In this point, it is very interesting and challenging to model and simulate the switching process in the switch.

1 Introduction

The multiphysics model of the crossconnect of the switch includes the micromirror with torsion rods, bottom electrodes and the surrounding gas (see Figure 1a). The incidence of the gas can be numerically modeled (and approximated) by the squeeze film damping effect [6]. Nevertheless, the Navier-Stokes equations in the conservative form should to be used for more precisely results. The voltage applied between micromirror and bottom electrodes determines the position of the micromirror. The step response of the micromirror on the applied voltage is highly oscillating due to absence of effective damping. Therefore, there is need for the design of an effective control system of the switch, or the effective damping, or both. The motion control of the micromirror is a nontrivial problem because of feedback of the position of the micromirror. There are many possibilities for realization of the feedback usually based on a capacitance sensing circuits. However, for reducing switching time, it is also possible to use an open-loop control when the effective damping is included.

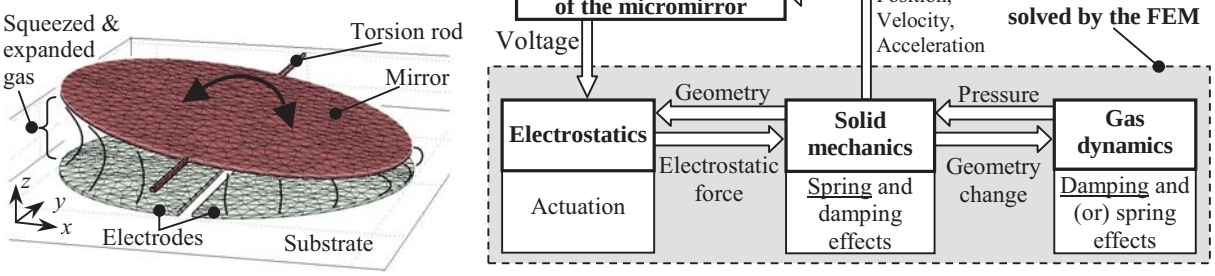

(a) Tilting of the micromirror in the crossconnect

(b) Multiphysics model of the crossconnect of the switch in block diagram with their interaction with control circuits

Figure 1. The model of the crossconnect of the switch

2 The model of the crossconnect

The multiphysics model is represented as a system of partial differential equations. The model consists of three parts (see Figure 1b), an electrostatics part described by the Poisson equation, a structural mechanics part described by the Newton equations, and a gas dynamics part decscribed by the Navier-Stokes equations. Simultaneous coupling between these three physical areas can model all essential processes in the crossconnect. The interaction is based on the coupled boundary conditions (e.g. through interactively acting forces on the boundaries, geometry conditions, etc.), which are computed in each time step. The model (represented through coupled partial differential equations) is discretized in the spatial and temporal domain. The spatial dicretization by standard Galerkin finite element method (standard GFEM) is used for electrostatics and solid mechanics; and then the Newmark method for time stepping is used only for solid mechanics. The temporal discretization by characteristic-Galerkin procedure and after that the standard GFEM for spatial discretization is used for gas dynamics because of convection-dominated problem.

2.1 Electrostatics

Electrostatic field within any media characterized by the permitivity ε is given by

$$-\nabla^{\mathrm{T}}\,\varepsilon\,\nabla\varphi = q_e\,, \tag{1}$$

where φ is electric potential, q_e is charge density and ∇ is the nabla operator defined as $\nabla = (\partial/\partial x,\ \partial/\partial y,\ \partial/\partial z)^{\mathrm{T}}$. After applying the weighted residual method to (1), performing a partial integration, Neumann conditions setting to zero, using approximation with standard nodal finite elements, using standard Galerkin method for choosing test functions and transformation into the discrete formulation we can rewrite (1) into the matrix form:

$$\mathbf{K}_{\varphi}\tilde{\boldsymbol{\varphi}} = \mathbf{f}_e\,, \tag{2}$$

where

$$\mathbf{K}_{\varphi} = \int_{\Omega}\varepsilon\left(\nabla\mathbf{N}_{\varphi}\right)^{\mathrm{T}}\nabla\mathbf{N}_{\varphi}\,\mathrm{d}\Omega\,,\quad \mathbf{f}_e = \int_{\Omega}\mathbf{N}_{\varphi}q_e\,\mathrm{d}\Omega\,. \tag{3}$$

For simplicity, the integration in above equation is written for whole domain Ω, but in real implementation of FEM the integration is divided into finite elements because of local support of each basis function. The integral over local domain Ω^e is evaluated by using the numerical Gauss quadrature rule. The tilde (~) is used for the identification of the nodal vector variable, and **N** for the basis (or shape) functions.

2.2 Solid mechanics

The Newton equations describing the dynamical behavior of mechanical system (for linear isotropic material) can be rewritten in the form:

$$\boldsymbol{\beta}^{T}\mathbf{E}\boldsymbol{\beta}\,\mathbf{u} + \mathbf{f} = \rho_M\,\frac{\partial^2\mathbf{u}}{\partial t^2}\,, \tag{4}$$

where **u** is the displacement vector, ρ_M is the mass density of the material, $\boldsymbol{\beta}$ is the differential operator, **E** is the elastic modulus matrix and **f** are external forces. In the above,

$$\boldsymbol{\beta} = \begin{pmatrix} \partial/\partial x & 0 & 0 \\ 0 & \partial/\partial y & 0 \\ 0 & 0 & \partial/\partial z \\ 0 & \partial/\partial z & \partial/\partial y \\ \partial/\partial z & 0 & \partial/\partial x \\ \partial/\partial y & \partial/\partial x & 0 \end{pmatrix},\quad \mathbf{E} = \begin{pmatrix} \lambda_L+2\mu_L & \lambda_L & \lambda_L & 0 & 0 & 0 \\ \lambda_L & \lambda_L+2\mu_L & \lambda_L & 0 & 0 & 0 \\ \lambda_L & \lambda_L & \lambda_L+2\mu_L & 0 & 0 & 0 \\ 0 & 0 & 0 & \mu_L & 0 & 0 \\ 0 & 0 & 0 & 0 & \mu_L & 0 \\ 0 & 0 & 0 & 0 & 0 & \mu_L \end{pmatrix}$$

with $\lambda_L = \dfrac{\nu E}{(1+\nu)(1-2\nu)}$ and $\mu_L = \dfrac{E}{2(1+\nu)}$,

where E is the Young's modulus of elasticity and ν is the Poisson constant. Similarly as in the electrostatics, the equation (4) can be rewritten in the matrix form:

$$\mathbf{M}_u\ddot{\tilde{\mathbf{u}}} + \mathbf{K}_u\tilde{\mathbf{u}} = \mathbf{f}_M\,, \tag{5}$$

where

$$\mathbf{M}_u = \int_{\Omega}\rho_M\,\mathbf{N}_u^{T}\mathbf{N}_u\,\mathrm{d}\Omega,\quad \mathbf{K}_u = \int_{\Omega}\mathbf{B}^{T}\mathbf{E}\,\mathbf{B}\,\mathrm{d}\Omega,\quad \mathbf{f}_M = \int_{\Omega}\mathbf{N}_u^{T}\mathbf{f}_V\,\mathrm{d}\Omega + \int_{\Gamma}\mathbf{N}_u^{T}\mathbf{f}_B\,\mathrm{d}\Gamma \tag{6}$$

with $\mathbf{f}_V$ being volume forces, $\mathbf{f}_B$ being surface forces on the boundary Γ; and matrix **B** defined by $\mathbf{B} = \boldsymbol{\beta}\mathbf{N}_u$.
The second term of $\mathbf{f}_M$ in equation (9) is evaluated only for elements on the boundary.

The Rayleigh damping model, in which the damping matrix $\mathbf{C}_u$ is computed via a linear combination of the mass matrix $\mathbf{M}_u$ and stiffness matrix $\mathbf{K}_u$ (i.e. $\mathbf{C}_u = \alpha_M\mathbf{M}_u + \alpha_K\mathbf{K}_u$), can include the damping effects in the solid mechanics part of the model. Thus, the equation (5) can be rewritten in the form:

$$\mathbf{M}_u\ddot{\tilde{\mathbf{u}}} + \mathbf{C}_u\dot{\tilde{\mathbf{u}}} + \mathbf{K}_u\tilde{\mathbf{u}} = \mathbf{f}_M\,, \tag{7}$$

and solved by the Newmark method (see e.g. [7]) for specified time-step value Δt.

2.3 Gas dynamics

The Navier-Stokes equations describe the motion of viscous fluid. All the essential features can be captured by set of three equations (mass, momentum and energy conservation) complemented by the universal gas law:

$$\frac{\partial\rho}{\partial t} = -\nabla^{T}\left(\rho\,\mathbf{v}\right) = \frac{1}{c^2}\frac{\partial p}{\partial t}\,, \tag{8}$$

$$\frac{\partial U_i}{\partial t} = -\nabla^{T}\left(\mathbf{v}U_i\right) + \nabla^{T}\begin{pmatrix}\tau_{ix} & \tau_{iy} & \tau_{iz}\end{pmatrix}^{T} - \frac{\partial p}{\partial i} - \rho_G g_i \quad \text{for } i = x, y, z \tag{9}$$

$$\frac{\partial(\rho E)}{\partial t} = \nabla^{T}\left(-\left(\rho_G E + p\right)\mathbf{v} + \boldsymbol{\tau}\mathbf{v} + k\nabla T\right), \tag{10}$$

$$\rho_G = \frac{p}{R_s T}, \tag{11}$$

where ρ_G is the density of the gas, c is the speed of sound, $\mathbf{v}$ is the gas velocity, U_i are components of $\mathbf{U}$, $\mathbf{U}$ is the flow flux given by $\mathbf{U} = \rho_G \mathbf{v}$, p is the gas pressure, $\rho_G g_i$ represents body forces and other source terms, τ_{ij} are the deviatoric stress components, k is the thermal conductivity, E is the specific energy, T is the absolute temperature and R_s is the specific gas constant.

In the above,

$$\boldsymbol{\tau} = \begin{pmatrix} \tau_{xx} & \tau_{xy} & \tau_{xz} \\ \tau_{yx} & \tau_{yy} & \tau_{yz} \\ \tau_{zx} & \tau_{zy} & \tau_{zz} \end{pmatrix} \quad \text{and} \quad \tau_{ij} = \mu\left(\frac{\partial u_i}{\partial j} + \frac{\partial u_j}{\partial i} - \frac{2}{3}\delta_{ij}\nabla^T \mathbf{v}\right), \;\; i, j \in \{x, y, z\} \tag{12}$$

where δ_{ij} is the Kronecker's delta (unity if $i = j$, 0 otherwise) and μ is the viscosity of the gas.

The following equations are useful to relate energy, temperature, velocity and speed of sound:

$$E = c_v T + \frac{1}{2}\mathbf{v}^T \mathbf{v}, \qquad c^2 = (\gamma - 1) c_p T. \tag{13}$$

We have used the characteristic-based split algorithm introduced by Zienkiewicz et al. [8–10] to discretize above equations in temporal domain. The four matrix equations after temporal and spatial discretization of equations (8–10) can be written in four steps as follow:

Step 1:

$$\Delta\tilde{\mathbf{U}}_i^* = -\mathbf{M}_v^{-1}\Delta t\left[\left(\mathbf{C}_v \tilde{\mathbf{U}}_i + \mathbf{K}_{\tau,i}\tilde{\mathbf{v}} - \mathbf{f}\right) - \Delta t\left(\mathbf{K}_v \tilde{\mathbf{U}}_i + \mathbf{f}_s\right)\right]^n, \tag{14}$$

for $i = x, y, z$, where

$$\begin{aligned} &\mathbf{M}_v = \int_\Omega \mathbf{N}_v^T \mathbf{N}_v d\Omega, \qquad \mathbf{C}_v = \int_\Omega \mathbf{N}_v^T \boldsymbol{\Psi}_v d\Omega, \qquad \mathbf{K}_{\tau,i} = \int_\Omega (\nabla N_v)^T \boldsymbol{\lambda}_i \mu \mathbf{Y} \mathbf{B} d\Omega, \\ &\mathbf{K}_v = -\frac{1}{2}\int_\Omega \boldsymbol{\Psi}_v^T \boldsymbol{\Psi}_v d\Omega, \qquad \mathbf{f}_s = -\frac{1}{2}\int_\Omega \boldsymbol{\Psi}_v^T \rho_G g_i d\Omega, \qquad \mathbf{f} = \int_\Omega \mathbf{N}_v^T \rho_G \, g_i \, d\Omega + \int_\Gamma \mathbf{N}_v^T \mathbf{n}\boldsymbol{\tau}_i \, d\Gamma, \end{aligned} \tag{15}$$

$$\boldsymbol{\Psi}_v = \nabla^T(\mathbf{v}\mathbf{N}_v) = \nabla^T \mathbf{v}\mathbf{N}_v + \mathbf{v}^T \nabla \mathbf{N}_v = \nabla^T \mathbf{N}_\mathbf{v}\tilde{\mathbf{v}}\mathbf{N}_v + (\mathbf{N}_\mathbf{v}\tilde{\mathbf{v}})^T \nabla \mathbf{N}_v, \tag{16}$$

$$\boldsymbol{\lambda}_x = \begin{pmatrix} 1 & 0 & 0 & 0 & 0 & 0 \\ 0 & 0 & 0 & 1 & 0 & 0 \\ 0 & 0 & 0 & 0 & 0 & 1 \end{pmatrix}, \quad \boldsymbol{\lambda}_y = \begin{pmatrix} 0 & 0 & 0 & 1 & 0 & 0 \\ 0 & 1 & 0 & 0 & 0 & 0 \\ 0 & 0 & 0 & 0 & 1 & 0 \end{pmatrix}, \quad \boldsymbol{\lambda}_z = \begin{pmatrix} 0 & 0 & 0 & 0 & 0 & 1 \\ 0 & 0 & 0 & 0 & 1 & 0 \\ 0 & 0 & 1 & 0 & 0 & 0 \end{pmatrix}, \tag{17}$$

$$\mathbf{Y} = \mathbf{I}_0 - \frac{2}{3}\mathbf{m}\mathbf{m}^T, \quad \text{where} \quad \mathbf{I}_0 = \begin{pmatrix} 2 & & & & & \\ & 2 & & & 0 & \\ & & 2 & & & \\ & & & 1 & & \\ & 0 & & & 1 & \\ & & & & & 1 \end{pmatrix}, \qquad \mathbf{m} = \begin{pmatrix} 1 \\ 1 \\ 1 \\ 0 \\ 0 \\ 0 \end{pmatrix}. \tag{18}$$

Step 2:

$$\Delta\tilde{\mathbf{p}} = \left(\mathbf{M}_p + \Delta t^2 \theta_1 \theta_2 \mathbf{H}\right)^{-1} \Delta t\left[\mathbf{G}\tilde{\mathbf{U}} + \theta_1 \mathbf{G}\Delta\tilde{\mathbf{U}}^* - \Delta t \theta_1 \mathbf{H}\tilde{\mathbf{p}}^n - \mathbf{f}_p\right], \tag{19}$$

where

$$\begin{aligned} &\mathbf{M}_p = \int_\Omega \mathbf{N}_p{}^T \left(\frac{1}{c^2}\right)^n \mathbf{N}_p d\Omega, \qquad \mathbf{G} = \int_\Omega (\nabla \mathbf{N}_p)^T \mathbf{N}_\mathbf{v} d\Omega, \\ &\mathbf{H} = \int_\Omega (\nabla \mathbf{N}_p)^T \nabla \mathbf{N}_p d\Omega, \qquad \mathbf{f}_p = \int_\Gamma \mathbf{N}_p^T \mathbf{n}^T \left[\tilde{\mathbf{U}}^n + \theta_1\left(\Delta\tilde{\mathbf{U}}^* - \Delta t \nabla\left(p^n + \theta_2 \Delta p\right)\right)\right] d\Gamma. \end{aligned} \tag{20}$$

Step 3:

$$\Delta\tilde{\mathbf{U}}_i = \Delta\tilde{\mathbf{U}}_i^* - \mathbf{M}_v^{-1}\Delta t\left[\mathbf{R}_i\left(\tilde{\mathbf{p}}^n + \theta_2 \Delta\tilde{\mathbf{p}}\right) + \frac{\Delta t}{2}\mathbf{P}_i \tilde{\mathbf{p}}^n\right], \tag{21}$$

for $i = x, y, z$, where

$$\mathbf{R}_i = \int_\Omega \mathbf{N}_v^T \frac{\partial}{\partial i}\mathbf{N}_p d\Omega, \qquad \mathbf{P}_i = \int_\Omega \left(\nabla^T(\mathbf{v}\mathbf{N}_v)\right)^T \frac{\partial}{\partial i}\mathbf{N}_p d\Omega = \int_\Omega \boldsymbol{\Psi}^T \frac{\partial}{\partial i}\mathbf{N}_p d\Omega. \cdot \tag{22}$$

Step 4:

$$\Delta\tilde{\mathbf{Z}} = -\mathbf{M}_E^{-1}\Delta t\left[\mathbf{C}_E \tilde{\mathbf{Z}} + \mathbf{C}_p \tilde{\mathbf{p}} + \mathbf{K}_T \tilde{\mathbf{T}} + \mathbf{K}_{\tau E}\tilde{\mathbf{u}} + \mathbf{f}_e - \Delta t\left(\mathbf{K}_{vE}\tilde{\mathbf{Z}} + \mathbf{K}_{vp}\tilde{\mathbf{p}}\right)\right]^n, \tag{23}$$

where

$$\mathbf{M}_E = \int_\Omega \mathbf{N}_E^T \mathbf{N}_E d\Omega, \quad \mathbf{C}_E = \int_\Omega \mathbf{N}_E^T \mathbf{\Psi}_E d\Omega, \quad \mathbf{K}_{\tau E} = \int_\Omega (\nabla \mathbf{N}_E)^T \boldsymbol{\tau} \mathbf{N}_\mathbf{v} d\Omega, \quad \mathbf{K}_T = \int_\Omega (\nabla \mathbf{N}_E)^T k \nabla \mathbf{N}_T d\Omega,$$
$$\mathbf{C}_p = \int_\Omega \mathbf{N}_E^T \mathbf{\Psi}_p d\Omega, \quad \mathbf{K}_{vp} - \frac{1}{2}\int_\Omega \mathbf{\Psi}_E^T \mathbf{\Psi}_p d\Omega, \quad \mathbf{K}_{vE} = -\frac{1}{2}\int_\Omega \mathbf{\Psi}_E^T \mathbf{\Psi}_E d\Omega, \quad \mathbf{f}_e = \int_\Gamma \mathbf{N}_E^T \mathbf{n}^T \left(\mathbf{t}^d \mathbf{v} + k \nabla T\right) d\Gamma, \tag{24}$$

where

$$\mathbf{\Psi}_E = \nabla^T (\mathbf{v} \mathbf{N}_E), \quad \mathbf{\Psi}_p = \nabla^T (\mathbf{v} \mathbf{N}_p) \quad \text{and} \quad \boldsymbol{\tau} = \mu \sum_{k=x,y,z} \boldsymbol{\lambda}_k \mathbf{Y} \mathbf{B} \tilde{\mathbf{v}} \boldsymbol{\alpha}_k \tag{25}$$

with

$$\boldsymbol{\alpha}_x = (1 \quad 0 \quad 0), \quad \boldsymbol{\alpha}_y = (0 \quad 1 \quad 0), \quad \boldsymbol{\alpha}_z = (0 \quad 0 \quad 1). \tag{26}$$

In the above equations, $\boldsymbol{\tau}_i = (\tau_{ix}, \tau_{iy}, \tau_{iz})^T$ is the traction corresponding to the deviatoric stress components; the superscript "n" indicates values in n-th time-step; Δt is the time-step increment; θ_1 and θ_2 are integration parameters; and $\tilde{\mathbf{Z}}$ contains the nodal values of $\rho_G E$.

It is necessary to mention that the gas flow velocity on the mirror boundary has to be the same as the velocity of the mirror. The mirror boundaries are subjected a load from the gas and from the electrostatic field. This load represents a sum of perpendicular pressure, viscous forces and electrostatic forces. The simulation of the coupled multiphysics model provides the velocity field, pressure distribution, and temperature distribution in the gas; electric field distribution; the mirror position; and the deformation and stress state in mechanical structure of the crossconnect.

3 Conclusion

Presented model and its solution by the finite element method are suitable for practical writing of the own simulation software, which is capable to model and simulate the described problem. The first disadvantage of the presented model is in the difficulty when it is coding in contrast to the model with concentrated parameters. The second disadvantage is a longer computational time for its simulation. Nevertheless, it provides a detailed view "into" the crossconnect and more precisely results by comparing the results of model with concentrated parameters. Thus it can be used for advanced micromirror design and optimization. Moreover, the model is universal in the sense that all electrostatic actuators can be modeled and simulated by this model, regardless of the shape of the actuator.

Acknowledgement
This work was supported by the VEGA Scientific Grant Agency of the Ministry of Education of the Slovak Republic and the Slovak Academy of Sciences S.G.A. grant No. 1/4081/07.

4 References

[1] Masaaki Kawai – Kazuyuki Mori – Tsuyoshi Yamamoto et al.: *Optical Components and Devices for Next-Generation Networks*. Fujitsu Sci. Tech. Joun., 42, 4, Oct. 2006, p.483–493.

[2] I. Plander, M. Stepanovsky. *All-optical Interconnection Networks: Optical Switch fabric for Core of the Optical Burst Switched Interconnection Network*. In: Proc. of the 9th Int. Conf. on Informatics – Informatics'2007. Bratislava: SSAKI, June 2007, pp. 36-40

[3] *Lucent's New All-Optical Router Uses Bell Labs Microscopic Mirrors*, Lucent Technologies, November 1999, [online: http://www.bell-labs.com/news/1999/november/10/1.html]

[4] Fernandez, A. – Staker, B.P. – Owens, W.E. et al.: *Modular MEMS design and fabrication for an 80×80 transparent optical crossconnect switch*. In: Proc. of SPIE. Optomechatronic Micro/Nano Components, Devices, and Systems. Vol. 5604, Oct. 2004, pp.208-217.

[5] Ryf, R. – Kim, J. – Hickey, J.P. et al.: *1296-port MEMS transparent optical crossconnect with 2.07 petabit/s switch capacity*. In: Optical Fiber Communication Conference and Exhibit, 2001. OFC 2001, Vol. 4, 17-22 March 2001, pp. PD28-1 - PD28-3.

[6] Pan, F. – Kubby, J. – Peeters, E. – Tran, A. T. – Mukherjee, S.: *Squeeze film damping effect on the dynamic response of a MEMS torsion mirror*, Technical Proceedings of the 1998 International Conference on Modeling and Simulation of Microsystems, 1998, pp.474-479.

[7] Kaltenbacher, M.: *Numerical Simulation of Mechatronic Sensors and Actuators*. Berlin (Germany): Springer-Verlag, 2004. 311 pp.

[8] Zienkiewicz, O.C. – Codina, R.: *Search for a general fluid mechanics algorithm*. Frontiers of Computational Fluid Dynamics, Eds. D.A. Caughey and M.M. Hafez. J. Wiley, New York, 101-113, 1995.

[9] Zienkiewicz, O.C. – Codina, R.: *A general algorithm for compressible and incompressible flow*, Part I. The split characteristics based scheme. Int. J. Num. Meth. Fluids, 20, 869-885, 1995.

[10] Zienkiewicz, O.C. – Taylor, R.L.: *The Finite Element Method: Fluid Dynamics*. 5th edition. Oxford: Butterworth-Heinemann, 2000. 334 pp. Vol.3.